Icarus 220 (2012) 339–347

Contents lists available at SciVerse ScienceDirect

Icarus

journal homepage: www.elsevier.com/locate/icarus

Sustainability of a subsurface ocean within Triton's interior

Jodi Gaeman [a,1], Saswata Hier-Majumder [a,b,*], James H. Roberts [c]

[a] Department of Geology, University of Maryland, College Park, MD 20742, USA
[b] Center for Scientific Computation and Applied Mathematical Modeling, University of Maryland, College Park, MD 20742, USA
[c] Applied Physics Laboratory, Johns Hopkins University, Laurel, MD 20723, USA

ARTICLE INFO

Article history:
Received 28 December 2011
Revised 4 May 2012
Accepted 6 May 2012
Available online 18 May 2012

Keywords:
Triton
Tides, Solid body
Neptune, Satellites

ABSTRACT

We present a study of coupled thermal and structural evolution of Neptune's moon, Triton, driven by tidal dissipation and radiogenic heating. Triton's orbital history likely involves capture from a binary system by Neptune, followed by a period of circularization. This work investigates Triton's evolution past its circularization. We examine the rate of ice shell growth as a function of different orbital eccentricities, in the presence of radiogenic heating. Tidal dissipation in the ice shell, proportional to orbital eccentricity squared, concentrates heating near the base, reducing the basal heat flux. As the growth of the ice shell is proportional to the basal heat flux, increased tidal heating creates a blanketing effect, reducing the rate of ice shell growth. Radiogenic heating from Triton's core is the other, more dominant, source of heat to the shell. Despite being several orders of magnitude higher than the tidal dissipation, radiogenic heating alone fails to sustain an ocean within Triton over 4.5 Ga. For orbital eccentricities of 5×10^{-7} and 3×10^{-5} it takes approximately 2 Ga and 3 Ga, respectively, to completely freeze the ocean. For higher values of orbital eccentricities, an ocean can be sustained in Triton's interior over 4.5 Ga. If Triton's history past circularization involves a slow decrease in orbital eccentricity to the current value, a thin, possibly NH_3-rich ocean exists beneath Triton's icy shell.

1. Introduction

Triton, an icy satellite of Neptune, shows evidence of recent geologic activity based on observations of its surface (Prockter et al., 2005). While the ages of many of the documented features remain unknown, the surface age of Triton is approximated between 10 and 100 Myr old (Schenk and Zahnle, 2007), suggesting recent geologic activity. The mechanism driving and sustaining such activity, however, is not clear.

One possible mechanism for Triton's activity, suggested by Prockter et al. (2005), is tidal diurnal stress, modulated by the eccentricity of Triton's orbit. Deformation via tidal activity, however, commonly occurs in planetary bodies orbiting at large eccentricities. Triton's current orbit is nearly circular (Ross and Schubert, 1990; McKinnon and Kirk, 2007), implying that tidal stresses are less likely to significantly deform the surface at present. Conversely, tidal heating likely played a significant role early in Triton's history.

Triton's relatively high density of 2065 kg/m^3 (McKinnon and Kirk, 2007), implies that a substantial part of the satellite's interior is likely composed of rock and possibly metal. Sustained internal activity, fueled by tidal dissipation and radiogenic heating may provide an alternative mechanism for surface activity on Triton (Ross and Schubert, 1990; Brown et al., 1991; Brown and Kirk, 1994; Ruiz, 2003). A few studies investigate the role of internal heating in the evolution, internal structure, and surface features of Triton.

Based on the density of Triton, and the likely abundance of radiogenic elements in Triton's core, Brown et al. (1991) estimated approximately $0.75–1.5 \times 10^{11}$ W of heat flow is generated by radioactive decay in the silicate part of Triton's core. Brown and Kirk (1994) demonstrated that this radiogenic heat can drive lateral heat transport and explain the surface distribution of volatiles. In a separate study, Ruiz (2003) calculated the thickness of the elastic lithosphere of Triton can be as low as 20 km beneath Raz Fossae, a pair of 15 km wide troughs.

Ross and Schubert (1990) developed a parametrized thermal–orbital evolution model of Triton incorporating tidal dissipation and radiogenic heating. Their model evaluates orbital evolution based on a k_2/Q ratio. In this model, k_2 is the degree-2 tidal Love number and Q is the dissipation factor, dependent on rheology, which, in turn is a function of temperature. Tidal dissipation in their model generated sufficient energy to cause large scale melting and the formation of a global ocean early in Triton's history. The parametrization, however, assumes a homogeneous internal structure of Triton.

Subsequent studies on coupled thermal–orbital evolution of terrestrial and icy satellites consider steady-state internal

* Corresponding author at: Department of Geology, University of Maryland, College Park, MD 20742, USA.
E-mail address: saswata@umd.edu (S. Hier-Majumder).
[1] Present address: Schlumberger, USA.

0019-1035/$ - see front matter © 2012 Elsevier Inc. All rights reserved.
http://dx.doi.org/10.1016/j.icarus.2012.05.006

structures (Hussmann and Spohn, 2004; Hussmann et al., 2006; Roberts and Nimmo, 2008; Meyer et al., 2010). Progressive thickening or thinning of the ice shell or crust was not dynamically incorporated in these studies, except the work of Robuchon and Nimmo (2011), where the thickness of the ice shell was tracked numerically. The steady-state model of Hussmann et al. (2006) indicate that a 135–190 km thick ocean likely exists in Triton's interior. The authors of this work, however, suggest that the evolution of tidal dissipation due to an increase in the thickness of the ice shell and variation of orbital eccentricity may exert important influence in the evolution of the icy satellites in general, and Triton in specific. This work addresses these issues in the coupled ice shell–ocean model with a time dependent ice shell thickness.

Progressive crystallization of a global ocean involves heat transfer between the coupled ice shell–ocean system, with a moving boundary or crystallization front. Coupled heat transfer and shell growth in such systems constitutes the Stefan class of problems (Caldwell and Kwan, 2004; Mitchell and Vynnycky, 2009; Tan and Zabaras, 2007; Hinze and Ziegenbalg, 2007; Hinze et al., 2009). In addition, tidal dissipation within this coupled system varies spatially and temporally. To study the retention of an ocean in Triton's interior, therefore, it is necessary to quantify the heat transfer in the coupled system with a robust description of tidal dissipation within Triton's interior.

This work couples the thermal, structural, and orbital evolution of Triton, assuming tidal dissipation occurs entirely within the ice shell, while radiogenic heating from the silicate fraction of the core is transmitted to the base of the ice shell by the convecting ocean. The goal of this study is to model the evolution of an ocean and to identify the conditions under which the ocean can be sustained over Triton's history.

In Section 2, we take a closer look at Triton's history. Section 3 outlines the governing equations and solution techniques involved in this work. We present the results of our numerical experiments in Section 4 and discuss the broader implications for coupling between tidal dissipation and crystallization of the ocean in Section 5.

2. Background

Triton's radius is approximately 1353 km, with an average density of approximately 2065 kg m^{-3} (McKinnon and Kirk, 2007). Models of the satellite's internal structure indicate that the satellite likely has a large silicate core, estimated to be approximately 950 km in radius. From limited observations, it is difficult to ascertain the structure of the icy portion of Triton. McKinnon and Kirk (2007) suggest that the satellite is differentiated given surface features indicative of melting and the distribution of various icy phases over the surface.

The Voyager mission imaged about 40% of Triton's surface. From this sampling of the surface, three types of terrains can be distinguished – volcanic plains, dynamic "cantaloupe" terrain, and polar caps (McKinnon and Kirk, 2007). Overall, the topographic relief is limited to 1 km, though most features are significantly smaller.

2.1. Composition

Analysis of Voyager mission data has provided a glimpse of Triton's chemical constituents, but not a detailed analysis of its composition. Observations of surface features and spectral analysis indicate that the surface composition of the satellite is predominantly H_2O with trace amounts of volatiles: N_2, CO,CO_2, and CH_4 (Brada and Clarke, 1997). About half of Triton's surface is composed of N_2 in solid solution with a minute amount of CO and CH_4. The other half is comprised of sections of either CO_2 or H_2O. These surface abundances, however, are not representative proportions of the satellite's interior (Schenk and Jackson, 1993). Models of presolar nebula chemical condensation lend an additional constraint to satellite composition. Recent estimates suggest up to 15% NH_3 within icy bodies in the outer Solar System (Choukroun and Grasset, 2007). The presence of NH_3-rich volatiles is significant in sustaining melt within an icy satellite as it decreases the solidus temperature (Choukroun and Grasset, 2007, 2010; Hogenboom et al., 1997; Hussmann et al., 2006). If an ocean on Triton formed approximately 4 Ga ago, the presence of volatiles may contribute significantly to whether or not the ocean can be sustained until present.

2.2. Orbital history

Triton is hypothesized to have originated in the Kuiper belt in a heliocentric orbit (McKinnon and Kirk, 2007), and subsequently captured into Neptune's orbit (Agnor and Hamilton, 2006). This hypothesis is based on the satellite's retrograde and inclined, circular orbit (Agnor and Hamilton, 2006). The mechanism of Triton's capture by Neptune is debated. One hypothesis suggests that Triton and a second body of similar size formed a binary system with the Sun (Agnor and Hamilton, 2006). As the binary's orbit approached Neptune, Triton was captured. An alternative hypothesis suggests that the satellite was captured during a close encounter with Neptune, or a series of close encounters, dissipating orbital energy via hydrodynamic drag (McKinnon and Leith, 1995). However, capture of Triton by the latter mechanism requires an unreasonably high gas density (Ćuk and Gladman, 2005) or a rather small window of time (Agnor and Hamilton, 2006).

Once captured, Triton's highly elliptical, heliocentric orbit circularized to its present, near zero eccentricity. At each passage of periapse, Neptune's gravity raised tides at the satellite's surface, dissipating energy within the satellite, and circularizing its orbit. Ross and Schubert (1990) show that this circularization process took place over 800 Ma since its capture. In an alternative approach, Ćuk and Gladman (2005) suggest that Triton's capture strongly perturbed the preexisting satellites, leading to collision and the formation of a debris disk. Subsequently, Triton's orbit evolved rapidly ($\leqslant 10^5$ yr) by interaction with this debris disk.

Deformation incurred by the satellite's orbital evolution would have dissipated a large amount of heat within Triton's interior, melting the icy layer of the satellite into a global ocean. McKinnon and Kirk (2007) approximate the dissipation of energy to be as much as 10^4 kJ kg^{-1}, enough to melt the satellite entirely.

Could an ocean, formed early during Triton's evolution, be sustained until present within Triton's interior? To determine if an ocean has survived, it is necessary to explore the coupled thermal–structural evolution. The purpose of this study is to evaluate the crystallization of a cooling ocean and to quantify the interaction between tidal dissipation, ice shell growth, and heat transfer in the shell. Our calculations start after the circularization event. As result, the orbital eccentricity remains constant throughout our calculations.

3. Model formulations

We study Triton's coupled thermal–structural evolution in the presence of tidal dissipation and radiogenic heating.

3.1. Tidal dissipation

We model Triton as a spherically-symmetric body with three primary layers: a silicate core of radius 950 km, overlain by an NH_3–H_2O ocean and H_2O ice shell with combined thickness of 403 km (see Table 1). Location of the ice shell–ocean interface

evolves with time based on the thermal structure (see Section 3.2 below). This interior structure is illustrated in Fig. 1. The ice shell is further subdivided radially into 100 incompressible Maxwellian layers with constant material properties within each layer. The assumption of incompressibility greatly reduces the computational cost and has negligible effects on the results (Moore and Schubert, 2000; Sabadini and Vermeersen, 2004).

Following Roberts and Nimmo (2008), we compute the spatially-variable tidal dissipation within the body. We use a propagator-matrix method (Sabadini and Vermeersen, 2004) to solve the equations of elastic spheroidal deformations, subject to tidal forcing to obtain the radially-varying displacements, stresses, potential, and potential stress (Roberts and Nimmo, 2008). We then follow the general approach of Tobie et al. (2005), in which we compute the stress and strain tensors from these radial functions and the laterally-varying tidal potential (Kaula, 1964). We use the correspondence principle (Biot, 1954) to extend this elastic solution to our viscoelastic Triton model, and compute the radially variable heating rate within Triton, integrated over an orbital cycle from the complex stress and strain rate (Schubert et al., 2001). A detailed description of the tidal dissipation calculation is provided by Roberts and Nimmo (2008). In our calculations, we use an ice shear modulus of 3.5 GPa and a viscosity of 1×10^{14} Pa s. We take the horizontal average of the 3D heating profile as a heat source in the parametrized coupled ice–ocean model described below. Our calculations do not consider dissipation in the ocean, which may play an important role in Triton's interior. A warmer, dissipating ocean will likely freeze at a rate slower than our calculations.

3.2. Coupled ice shell–ocean model

Secular cooling of Triton leads to continual freezing of the ocean and propagation of the ice-fluid interface from the surface towards the ocean-core boundary. Determination of the thermal structure in Triton's interior, and computation of the rate of freezing belongs to the Stefan class of problems (Caldwell and Kwan, 2004; Mitchell and Vynnycky, 2009; Tan and Zabaras, 2007; Hinze et al., 2009). The schematic diagram in Fig. 1 outlines the fundamental energy balance under this condition. This calculation does not incorporate convection in the ice shell. Robust numerical methods for studying convective heat transport in a domain with a moving boundary are currently under development (Hinze et al., 2009; Robuchon and Nimmo, 2011), and are outside the scope of this article. We present a discussion on the uncertainties in heat transfer associated with the neglect of convection in Section 5.2.

Consider the incremental growth of the ice shell over a small time period δt. As the ocean freezes to add the incremental layer, energy is released via the loss of latent heat of crystallization. In addition, decay of radioactive elements in the silicate core also release heat, which is transferred by turbulent convection in the ocean, marked as $q_{rad}(t)$ in the diagram. The energy from these two source must be transferred through heat conduction in the ice shell. The efficiency of conductive heat transport in the shell, therefore, limits the rate at which the freezing front propagates. Besides the conductivity of ice and latent heat, the presence of additional heat sources, such as tidal dissipation and radiogenic heating, also contribute to the rate of propagation of the freezing front. We model this coupled process as the Stefan problem with two unknowns, the ice shell temperature, $T_{ice}(z,t)$, and the ice shell thickness, $h(t)$. First, conservation of energy within the conductive ice shell leads to

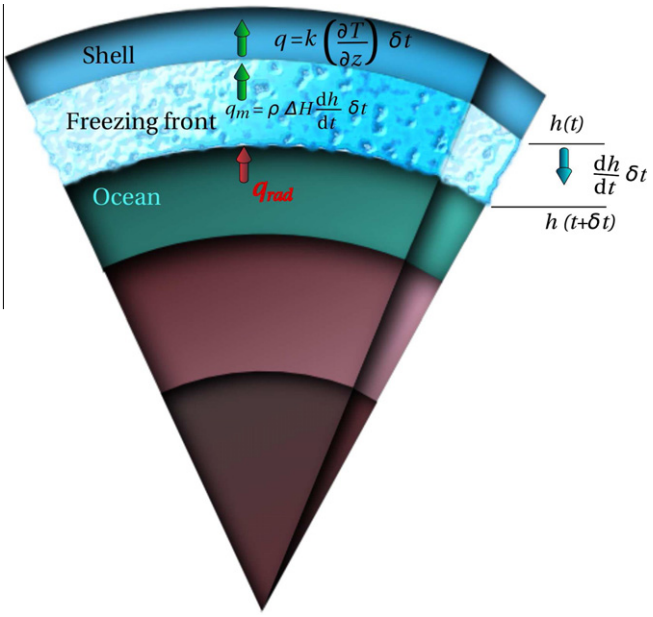

Fig. 1. A schematic outline demonstrating the heat transfer in a crystallizing ocean, the Stefan problem. The freezing front advances by the amount $(dh/dt)\delta t$, over a small increment of time δt. The latent heat released by freezing must be conducted through the ice shell. The instantaneous position of the front is given by $h(t)$.

$$\frac{\partial T_{ice}(z,t)}{\partial t} = \frac{k}{\rho_{ice} c_p}\frac{\partial^2 T_{ice}(z,t)}{\partial z^2} + \frac{\psi_c(z,t)}{\rho_{ice} c_p}, 0 \leqslant z \leqslant h(t), \tag{1}$$

where $T_{ice}(z,t)$ is temperature of the ice shell, t is time, z is depth, ρ_{ice} is the density, c_p is the specific heat capacity, k is the thermal conductivity, and $\psi_c(z,t)$ is the tidal dissipation within the ice shell.

We need an additional equation to solve for the unknown ice shell thickness $h(t)$. This ODE arises from the balance between latent heat of crystallization, ΔH, radiogenic heat flux, $q_{rad}(t)$, and conductive heat flux within the freezing front, as depicted in Fig. 1, given by,

$$\rho_{ice}\Delta H \frac{dh(t)}{dt} = k\left(\frac{\partial T_{ice}(z,t)}{\partial z}\right)_{z=h(t)} - q_{rad}(t)|_{z=h(t)}. \tag{2}$$

The left hand side of Eq. (2) depicts the freezing rate of the ocean or the growth rate of the ice shell. The right hand side arises from the net basal heat flux. The total radiogenic heat flow is a sum of contribution of radiogenic heating from the four major radiogenic elements, ^{238}U, ^{235}U, ^{232}Th, and ^{40}K. The radiogenic heat flux at time t is given by,

$$q_{rad}(t)|_{z=h(t)} = \frac{V_{sil}\rho_{sil}}{4\pi(R_c + H - h)^2}\sum_i c_i^0 p_i H_i \exp\left(\frac{(t_0 - t)\ln 2}{\tau_i}\right), \tag{3}$$

Table 1
Abundance of radiogenic elements in the silicate core. See text for source of data.

Isotope	Fraction (p_i)	Heat production (H_i) (W kg^{-1})	Half life (τ_i) (yr)	Concentration (c_i^0) (kg/kg)
^{238}U	9.93×10^{-1}	94.65×10^{-6}	4468×10^6	8.40×10^{-9}
^{235}U	7.20×10^{-3}	568.70×10^{-6}	704×10^6	8.40×10^{-9}
^{232}Th	1.00	26.38×10^{-6}	$14{,}030 \times 10^6$	30.90×10^{-9}
^{40}K	1.28×10^{-4}	29.17×10^{-6}	1277×10^6	530×10^{-6}

where the V_{sil} is the volume and $\rho_{sil} = 3300$ kg m^{-3} is the density of the silicate fraction of the core, R_c is the radius of the core, H is the depth to core, c_0^i is the total abundance of the radioactive element, p_i is the fractional abundance of the ith isotope within the element, H_i is the heat generated per unit mass, τ_i is the half life of the species in years, $t_0 = 4.567 \times 10^9$ years, and t is the time in years. The silicate volume of the core was calculated assuming a metallic inner core of 600 km radius (McKinnon and Kirk, 2007). The parameters p_i, H_i, τ_i, and c_0^i are listed in Table 1. The first column (p_i) is taken from Eq. (4.1.42) of Schubert et al. (2001). The second and third columns (H_i and τ_i) are taken from Table 3 of Robuchon and Nimmo (2011). Concentration of radioactive elements, c_0^i, were obtained from Table 3 of Lodders (2003).

The numerical solution building technique for the coupled Eqs. (1) and (2) is discussed in Appendix A.

Finally, the temperature distribution within the ocean underlying the shell is given by the multiphase adiabatic gradient

$$\frac{dT_m}{dz} = \frac{\alpha' g T_m}{c_p'}, \tag{4}$$

where c_p' is the effective heat capacity, g is gravity, and α' is the effective coefficient of thermal expansion. The effective quantities can be determined from the end member compositions using the relations (Solomatov, 2007),

$$\alpha' = \alpha + \frac{\Delta\rho}{\rho(T_{liq} - T_{sol})}, \tag{5}$$

$$c_p' = c_p + \frac{\Delta H}{(T_{liq} - T_{sol})}, \tag{6}$$

where ΔH is the latent heat of crystallization. Once the thickness of the ice shell is calculated, we calculate the thermal profile within the ocean by numerically integrating Eq. (4) using the fourth order Runge–Kutta algorithm.

3.3. Nondimensionalization

In the coupled ice shell–ocean model, we nondimensionalize the temperature by the surface solidus temperature in the NH_3–H_2O system, T_{sol}; depth by the depth to the core, H; time by a thermal conductive time scale, $t_0 = \rho_{ice} c_p H^2/k$, tidal heating by $\rho_{ice} c_p T_{sol}/t_0$, and radiogenic heat flux by $k\Delta H/(c_p H)$ to obtain the nondimensional differential equations for the unknowns $T_{ice}(z,t)$ and $h(t)$,

$$\frac{\partial T_{ice}(z,t)}{\partial t} = \frac{\partial^2 T_{ice}(z,t)}{\partial z^2} + \psi_c(z,t), \tag{7}$$

$$\frac{dh(t)}{dt} = \mathcal{S}t\left(\frac{\partial T_{ice}(z,t)}{\partial z}\right)_{z=h(t)} - q_{rad}(t)|_{z=h(t)}. \tag{8}$$

The dimensionless Stefan number in Eq. (8), defined as

$$\mathcal{S}t = \frac{T_{sol} c_p}{\Delta H}, \tag{9}$$

signifies the ratio between the energy required to change the temperature and latent heat of crystallization. As seen from Eq. (8), the freeze rate dh/dt is directly proportional to $\mathcal{S}t$. Using the values listed in Table 2, we obtain $\mathcal{S}t = 1.87$, which was used in our numerical simulations.

Boundary conditions for the coupled energy conservation and ice shell growth Eqs. (7) and (8) are

$$T_{ice}(0,t) = T_{surf}, \tag{10}$$

$$T_{ice}(h(t),t) = T_{sol}, \tag{11}$$

$$T_{ice}(z,0) = T_{sol}. \tag{12}$$

The initial condition for ice shell thickness h is given by,

$$h(0) = 0. \tag{13}$$

4. Results

As Triton cools, the growth rate of the ice shell depends on the spatially varying tidal dissipation, radiogenic heat flux, and thermal conduction through the ice shell. The following subsections outline the numerical results for these processes.

4.1. Tidal dissipation within the ice shell

As the ocean crystallizes, tidal dissipation in the ice shell plays a crucial role in the subsequent thermal and structural evolution. On the one hand, the magnitude and spatial distribution of tidal dissipation within the uniform ice shell influence the heat transfer within the shell. On the other, thickness of the ice shell influences the extent of tidal heating in the shell for a given orbital eccentricity. These aspects of the two-way coupling between tidal heating and structural evolution are depicted in the plots in Figs. 2 and 3.

Tidal dissipation is distributed unevenly through the ice shell. The ocean decouples the ice shell from the core, concentrating deformation near the base of the ice shell. Consequently, tidal dissipation preferentially warms the bottom of the shell. The series of thermal profiles on both Fig. 2a and b demonstrate such a pattern. The depth to the bottom of each curve in Fig. 2 marks the corresponding thickness of the ice shell. In addition, average tidal dissipation between the two cases in Fig. 2a and b vary by approximately four orders of magnitude. The orbital eccentricities, annotated in the plots, vary by nearly two orders of magnitude between the two cases. Tidal dissipation is proportional to the square of orbital eccentricity (Roberts and Nimmo, 2008). Consequently, after capture and circularization of Triton's orbit, the magnitude of tidal dissipation in the shell must have decreased significantly.

The amount of tidal dissipation also depends on the thickness of the shell. The curves in the plot in Fig. 3 compare the mean volumetric tidal heating within the ice shell as a function of shell thickness. The orbital eccentricity corresponding to each curve are displayed in the legend. Tides deform thin shells more easily, resulting in a larger magnitude of tidal dissipation. As the shell thickens, it becomes progressively more difficult to deform, reducing the tidal dissipation in the shell. When the ocean is completely frozen, the shell is no longer decoupled from the core. As a result, the resistance to tidal deformation increases substantially, as evidenced by the sharp drop in the two curves corresponding to the lowest eccentricities. A similar trend is also reflected in Fig. 2, as the dissipation profiles shift to lower magnitudes as the shells thicken.

4.2. Thermal and structural evolution

Tidal dissipation in the icy shell preferentially warms the bottom of the shell, reducing the basal heat flux. At higher orbital eccentricities, this effect is more prominent. Reduction in the basal heat flux, in turn, reduces the efficiency of transport of latent heat of crystallization, slowing down the rate of shell growth. Consequently, the ice shell acts as a warm, tidally heated blanket over the freezing ocean and slows down the rate of freezing. In this section we present data from our numerical simulations outlining various aspects of this blanketing effect. As the following plots demonstrate, this effect influences the freezing rate even at small orbital eccentricities $O(10^{-5})$.

The thermal structure within Triton's evolving interior is influenced by the orbital eccentricity. The plots in Fig. 4 depict the thermal profile and tidal dissipation profile at three different time steps. The legends on the curves indicate time in Ma since the onset of crystallization. The dashed part of each curve represents the adiabat within the ocean. Solid curves in the left panels represent

Table 2
Value of constants used in the parametrized turbulent cooling and coupled shell–ocean cooling models.

Symbol	Description	Units	Reference
R	Radius of Triton	1353 km	McKinnon and Kirk (2007)
R_c	Radius of core	950 km	McKinnon and Kirk (2007)
H	Depth to core	403 km	
g	Gravitational acceleration	0.8 m s^{-2}	McKinnon and Kirk (2007)
V_{sil}	Volume of the silicate fraction of core	1.79×10^{17} m^3	(see Section 3.2)
T_{sol}	Solidus temperature	176 K	Hogenboom et al. (1997)
T_s	Surface temperature	38 K	McKinnon and Kirk (2007)
k	Thermal conductivity	4.3 W m^{-1} K^{-1}	Slack (1980)
c_p	Specific heat capacity	1400 J K^{-1} kg^{-1}	Feistel and Wagner (2006, Fig 5a)
α	Coefficient of volume expansion	5×10^{-5} K^{-1}	Feistel and Wagner (2006, Fig 3a)
ρ_{ice}	Density of ice	917 kg m^{-3}	Hogenboom et al. (1997)
ρ	Density of fluid	946 kg m^{-3}	Hogenboom et al. (1997)
ΔH	Latent heat of crystallization	1.32×10^5 J kg^{-1}	Chan and Giauque (1964)
$\mathcal{S}t$	Stefan number	1.87 (dimensionless)	

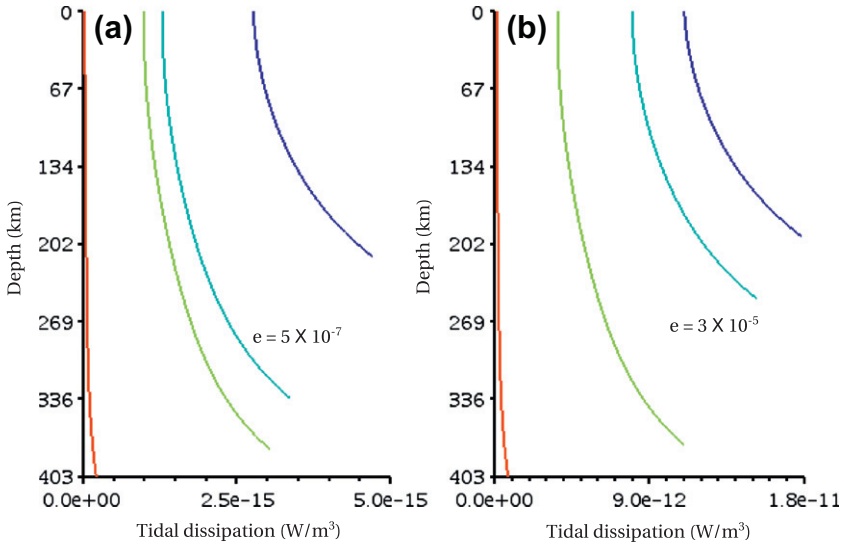

Fig. 2. Vertical distribution of tidal dissipation within the ice shell. Each curve terminates at the bottom of the ice shell. The two plots correspond to eccentricities of (a) 5×10^{-7} and (b) 3×10^{-5}.

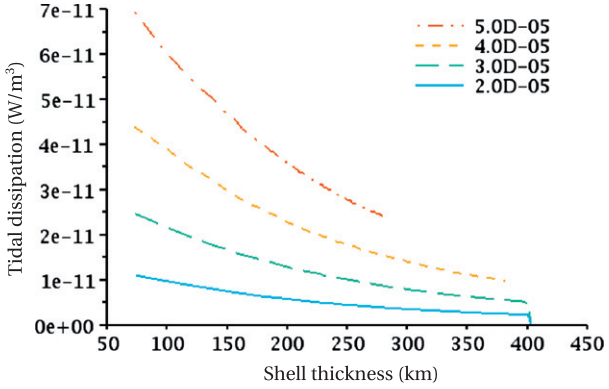

Fig. 3. Variation of average tidal dissipation with the thickness of the icy shell for various orbital eccentricities. Legends in the plot indicate the orbital eccentricity corresponding to each curve.

the conductive thermal profiles within the shell. Depth to the bottom of each curve in the right panels represent the thickness of the shell. The top and bottom panels in plots in Fig. 4 correspond to orbital eccentricities of 5×10^{-7} and 5×10^{-5}, respectively. Tidal dissipation in the latter case is higher by a factor of 1×10^4. In the first case, the ocean is almost completely frozen by 1.8 Ga, while in the second case, a nearly 130 km thick ocean remains after 4.5 Ga.

Numerical solutions to the Stefan problem allow us to calculate the growth of Triton's ice shell as a function of time for different eccentricities. The results from these simulations are plotted in Fig. 5a and b. The plot in Fig. 5a also overlays the current estimate of the depth to Triton's core as the broken, horizontal line. The legends on the plots indicate orbital eccentricity. Even an orbital eccentricity of 4×10^{-5} is able to prevent complete freezing of Triton's interior over a period of 4.5 Ga. For orbital eccentricities higher than 4×10^{-5}, the ocean never completely freezes over 4.5 Ga. The plots in Fig. 5b also indicate that within the first 500 Ma, the freeze rate dh/dt, reduces to less than half the original value.

From the numerical simulations, we evaluate the surface heat flux and the conductive heat flux at the base of the ice shell as a function of time for various values of orbital eccentricity in Fig. 6. Comparison between these two plots, and different curves within each plots demonstrate the tidal blanket effect. The heat flux near the surface is higher than the basal heat flux. Our calculated value of surface heat flux varies between 2.4 and 4.0 m W/m^2, similar to the estimated heat flux of 3.3–6.6 m W/m^2 of Brown et al. (1991) and 3.02 m W/m^2 of Hussmann et al. (2006). These

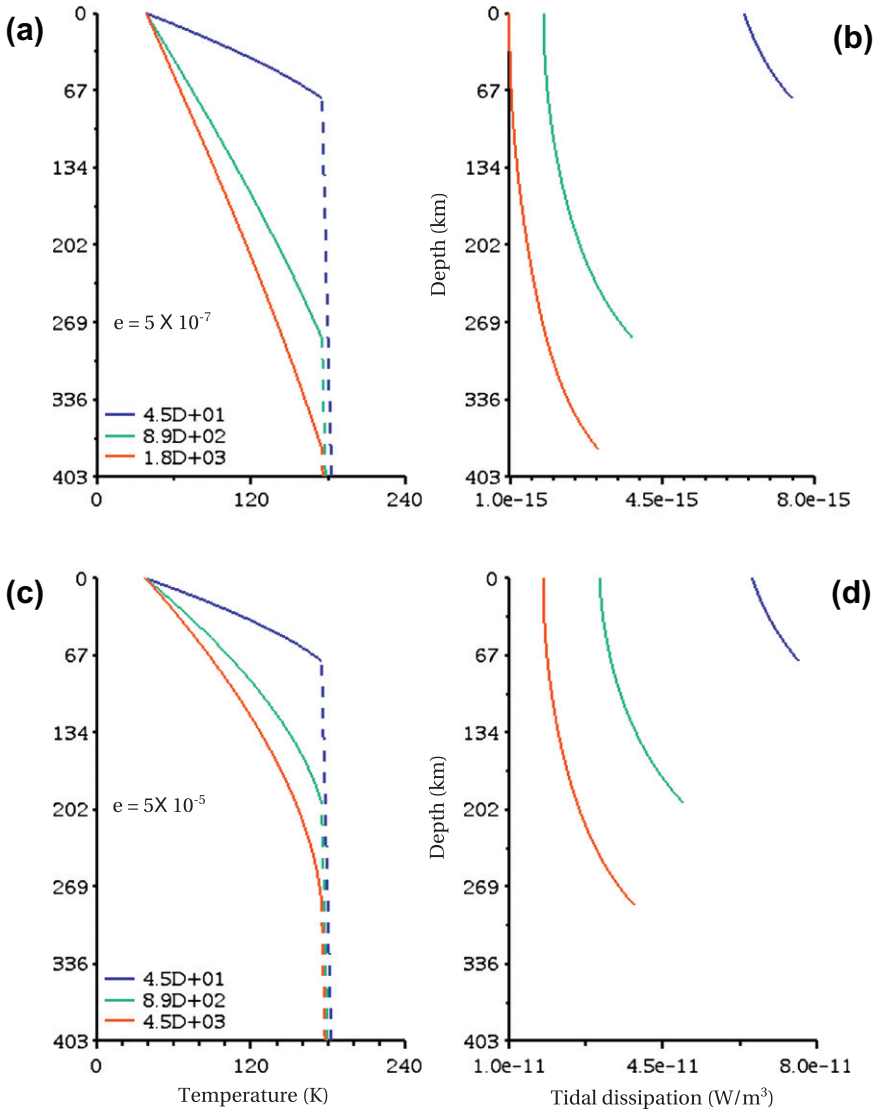

Fig. 4. Coupled thermal and structural evolution in an ice shell–ocean system. (a) Successive thermal profiles within Triton's interior. Solid and broken parts of the curves indicate the thermal profile within the ice shell and the ocean, respectively. Legends for each curve corresponds to time in Ma since the onset of crystallization. The orbital eccentricity is 5×10^{-7}. (b) Evolution of tidal dissipation within the shell. The time intervals and eccentricity are the same as in figure (a). The bottom of the curves correspond to the bottom of the icy shell. (c) Thermal profile within the shell–ocean system for an eccentricity of 5×10^{-5}. Legends are similar to (a). (d) Tidal heating within the ice shell. The orbital eccentricity is the same as in (c).

values are lower than the estimated 44–57 m W/m^2 surface heat flux of Ruiz (2003) for a water–ice lithosphere. The basal heat flux in Fig. 6b is purely conductive. The magnitude of the basal heat flux always remains lower at higher orbital eccentricities. As demonstrated in Fig. 2 and the series of heating profiles in Fig. 4, the base of the ice shell is preferentially warmed by tidal heating. Since the shell–ocean interface is held at a constant temperature, higher dissipation at the base of the shell reduces the thermal gradient. As a result, higher orbital eccentricities lead to lower basal heat fluxes, as seen in the curves in Fig. 6b.

Radiogenic heating in our calculation agrees well with the estimate for Triton's radiogenic heat flow by Brown et al. (1991). In Fig. 7a, radiogenic heat flow is plotted as a function of time. Using chondritic abundance of the radiogenic elements for the outer silicate core of Triton, the radiogenic heat flow varies between 3×10^{11} and 3×10^{10} W. For comparison, the estimate of radiogenic heat flow from Brown et al. (1991) is also overlain on the plot.

The curves in Fig. 7b compares the evolution of tidal heating as a function of time, for three different values of orbital eccentricity. The total tidal heating increases as the shell volume increases, despite a decrease in volumetric tidal heating with an increase in shell volume as depicted in Fig. 3. The curve for orbital eccentricity of 2×10^{-5} displays a sharp drop in tidal heating around 2500 Ma, corresponding to complete crystallization of the ocean. As the frozen ocean locks with the silicate core, tidal dissipation drops sharply. In the curve labeled 1×10^{-4}, the shell thickness becomes nearly constant after the first few hundred million years, as a result, tidal heating remains constant through the rest of the simulation also. As the shell continues to grow through the entire simulation, tidal heating constantly increases for an orbital eccentricity of 4×10^{-5}.

Of the two energy sources, radiogenic heating is at least six orders of magnitude higher than tidal heating in our calculations. Yet the modest tidal heating makes a difference in the rate of freezing. This seemingly paradoxical effect can be explained by the uneven spatial distribution of tidal heating over a relatively small region. We discuss this effect in detail in the following section.

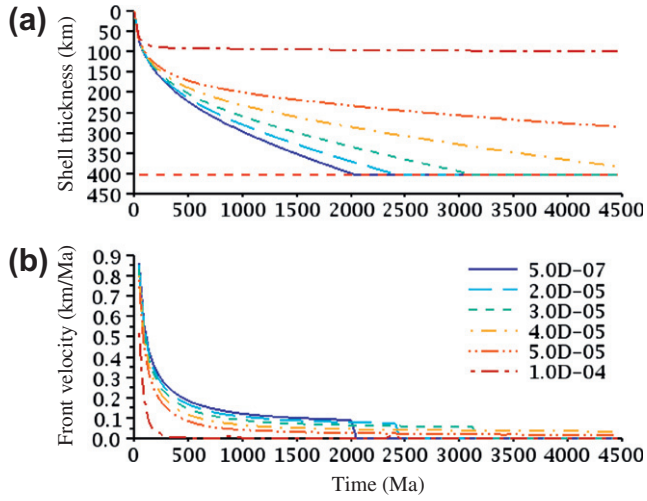

Fig. 5. Freezing rate of the ocean. (a) Thickness of the icy shell in km, and (b) velocity of the freezing front as a function of time in Ma. The legends on the plots correspond to different values of orbital eccentricity. The broken horizontal line in (a) represents the current estimate of the depth to the core.

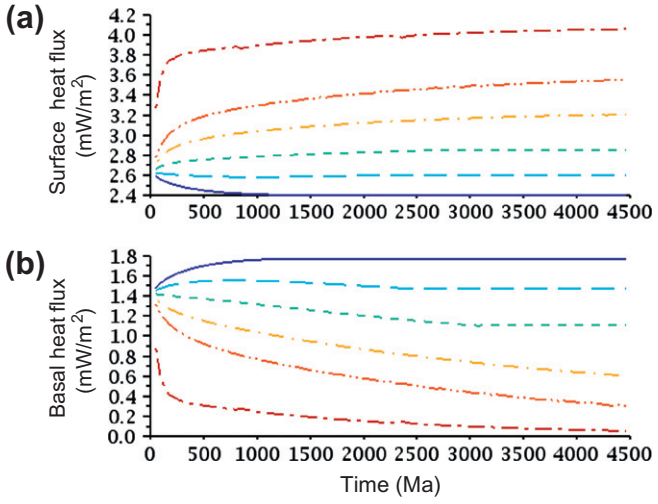

Fig. 6. (a) Surface and (b) basal heat conductive fluxes in the freezing ice shell as a function of time. Different curves on the plot correspond to different orbital eccentricities. The legends, omitted to avoid cluttering, are identical to those in Fig. 5b.

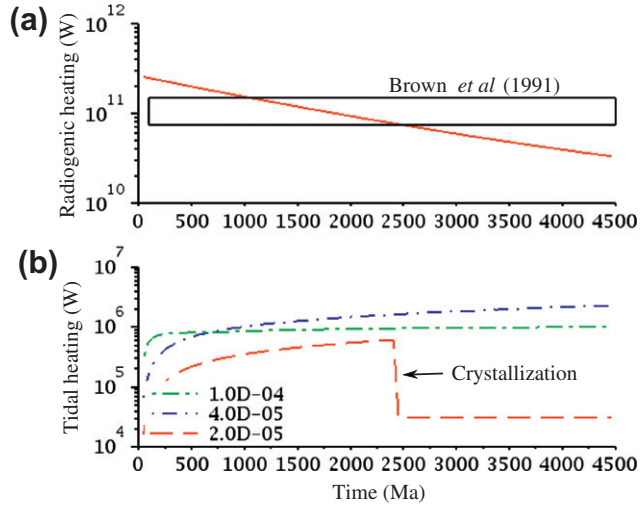

Fig. 7. (a) Radiogenic heating in Triton's silicate core as a function of time. The horizontal box indicates the range of total radiogenic heating of Triton (0.75–1.5 $\times$ 10^{11} W) estimated by Brown et al. (1991). (b) Tidal heating in the ice shell as a function of time for three different orbital eccentricities. The annotation in the curve for an orbital eccentricity of 2 $\times$ 10^{-5} represents complete crystallization of Triton's internal ocean.

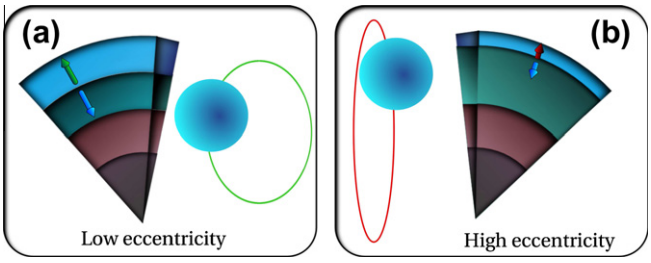

Fig. 8. A schematic diagram outlining the tidal blanketing effect in the crystallizing ice shell. Lengths of the upward pointing red and green arrows correspond to the magnitudes of basal heat flux arising from the tidal dissipation. Similarly, lengths of the downward pointing blue arrows represent the magnitudes of ice shell growth for the two cases. As indicated in the cartoon, higher tidal dissipation corresponds to lower basal heat flux and a reduced rate of ice shell growth. (For interpretation of the references to color in this figure legend, the reader is referred to the web version of this article.)

5. Discussion

5.1. Tidal blanketing

The modest amount of tidal heating in Triton's ice shell plays an insignificant role in comparison to radiogenic heating in raising the overall temperature of the satellite. Despite the modest magnitude, tidal heating plays a significant role in the energy transfer near the base of the ice-shell. As evident from the plot of shell thickness as a function of time in Fig. 5a, radiogenic heating fails to sustain the ocean in Triton's interior over a period of 4.5 Ga for the lowest orbital eccentricities.

Tidal dissipation in the growing ice shell insulates the underlying, crystallizing ocean, reducing the basal heat flux and delaying ice shell growth. The overall effect of a dissipative ice shell is to provide a thermal blanket atop the ocean. We term this the 'tidal blanketing' effect. The cartoon in Fig. 8 summarizes some of the key processes associated with tidal blanketing. First, we notice that the magnitude of tidal dissipation is higher for higher orbital eccentricity. As shear decoupling between the shell and the ocean concentrates the tidal heating near the bottom of the shell, at higher orbital eccentricities, the bottom of the ice shell is warmer. Since the base of the ice shell is fixed at the solidus temperature, warming of the lower part by tidal dissipation reduces the thermal gradient and thus the basal heat flux. The growth rate of the ice shell, derived from the Stefan problem, is proportional to the basal heat flux within the ice shell. Consequently, the growth of ice shell by crystallization is impeded. Since high eccentricity of the orbit leads to larger tidal dissipation, the tidal blanketing effect is stronger at higher eccentricities.

5.2. Sources of uncertainty

In this section, we discuss the sources of uncertainty in our models. These uncertainties arise from ignoring convection in the icy shell and the amount of radiogenic heating.

In our model, we treat the ice shell as a purely conductive lid. As Triton's ice shell thickens with time, however, convection becomes more efficient in transporting heat across the ice shell. The curves

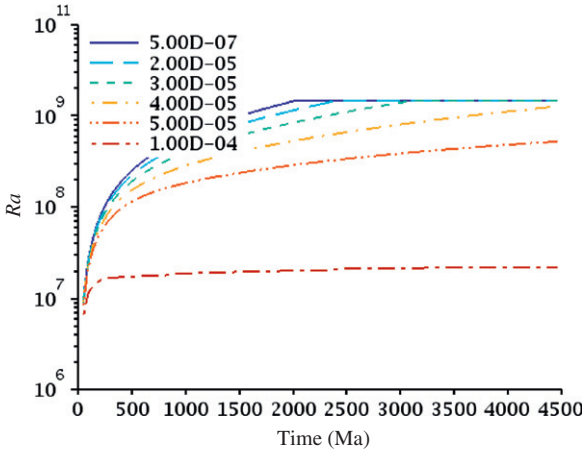

Fig. 9. Evolution of the nondimensional Rayleigh number with time. The legends on the plots indicate orbital eccentricity. The critical Rayleigh number, Ra_c is $\mathcal{O}(10^7)$ when the viscosity of ice depends strongly on the temperature (Robuchon and Nimmo, 2011).

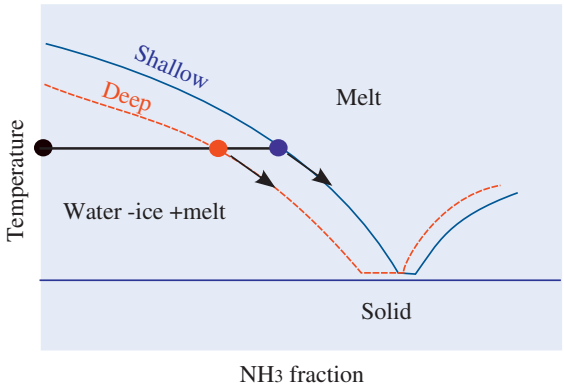

Fig. 10. A schematic melting diagram in the NH_3-H_2O system, modified from Hogenboom et al. (1997). The red and blue dots indicate the composition of a in equilibrium with an H_2O–ice phase at deep and shallow levels, respectively. (For interpretation of the references to color in this figure legend, the reader is referred to the web version of this article.)

in Fig. 9 plot the evolution of the Rayleigh number as a function of time for different eccentricities. The convective threshold for an isoviscous fluid layer, $Ra \sim 10^3$ is reached almost instantaneously, as the curves indicate. For a strong temperature dependent ice rheology, the critical Rayleigh number in a spherical shell is much higher. Robuchon and Nimmo (2011) estimate a critical Rayleigh number of 4×10^7 for an ice shell. This critical Rayleigh number also, is exceeded within the first few hundred million years for all cases except for the orbital eccentricity of 1×10^{-4}, which remains nearly critical.

We can estimate the ratio between convective and conductive heat flux, the Nusselt number *Nu*, for the calculated Rayleigh numbers using the following scaling relation (Schubert et al., 2001, Eq. 13.2.4),

$$Nu = \left(\frac{Ra}{Ra_c}\right)^{1/3}, \tag{14}$$

where *Ra* and Ra_c are the Rayleigh and the critical Rayleigh numbers, respectively. Using $Ra_c = 4 \times 10^7$ and $Ra = 1.5 \times 10^9$, the maximum value, we obtain $Nu = 3.34$, a relatively modest ratio between convective and conductive heat flux.

Thermal convection in the ice shell will likely influence the magnitude of shell growth less than it will influence the lateral variation of the growth rate. While convection within the ice shell will modify the thermal profile within the ice shell, conduction will still dominate at the thermal boundary layer at the ice shell–ocean boundary. The rate of ocean freezing will still be controlled by heat conduction within the conductive thermal boundary layer. Given the modest value of *Nu* in scaling relation (14), the magnitude of convective heat flux will be similar to the conductive heat flux in this study. Convection within the ice shell, however, will lead to lateral variation of heat flux by formation of upwellings and downwellings. The spatial variation in basal heat flux will be reflected in a spatial variation of ice shell growth rate. In regions of high basal heat flux, such as the base of thermal plumes, the ice shell thickness will be higher. Future studies incorporating thermal convection in the ice shell coupled with a Stefan-type shell growth rate will help understanding the nature of spatially varying ice shell growth under these conditions.

The second source of uncertainty in our calculation arises in the estimate of radiogenic heating. We assume the radiogenic elements, of chondritic abundance, are concentrated in a silicate-rich, rocky outer core. Following McKinnon and Kirk (2007), we assume the metallic inner core has a radius of 600 km. Ross and Schubert (1990) argue that during the circularization of Triton, enough heat was generated to melt the entire planet. We assume such widespread melting of the planet likely led to the segregation of the metallic core and concentration of the radiogenic elements into the silicate outer part. While our estimated total radiogenic heat flow is similar to the estimated heat flow by Brown et al. (1991), a larger amount of radiogenic heating will result in a thinner ice shell and a larger ocean mass.

5.3. Composition of the ocean

One consequence of crystallization of the ocean is progressive change in the composition of the fluid. As illustrated in the cartoon in Fig. 10, the concentration of ammonia within the ocean increases with progressive crystallization. Since the shell of Triton is predominantly composed of water–ice, it is likely that the bulk composition lies on the H_2O side of the eutectic curve in Fig. 10. As the ocean cools and crystallization progresses, composition of the liquid evolves along the liquidus curves, in the direction indicated by the arrows in the diagram. One important consequence of such progressive enrichment of the ocean in NH_3 is that the liquid becomes denser than the crystallizing H_2O–ice (Hogenboom et al., 1997). Progressive enrichment of the liquid in NH_3 also reduces its viscosity (Hogenboom et al., 1997), enhancing gravitational drainage of trapped pore fluid within the freezing front. As a consequence, a thin layer of NH_3-rich fluid can be rendered dynamically stable beneath the ice shell. Although the liquidus is shifted towards the H_2O end of the phase diagram at higher pressures, the trend of compositional enrichment still exists. Thus with sufficient tidal blanketing, it is possible to create and retain an NH_3-rich fluid layer at the base of the ice shell.

6. Conclusions

Our coupled tidal-thermal evolution model indicates that radiogenic heating, tidal dissipation, and structural evolution of Triton is closely related. Triton's history immediately after orbit circularization and widespread melting is likely marked by a short-lived turbulent cooling regime, followed by a slower, coupled ice shell–ocean evolution phase. The growth of the ice shell is influenced by tidal blanketing. At high orbital eccentricities, tidal dissipation warms up the bottom of the ice shell, reducing the basal heat flux and slowing the growth of the ice shell. For orbital eccentricities as

low as 4×10^{-5}, Triton's interior ocean cannot be completely crystallized over a period of 4.5 Ga.

Acknowledgments

S.H.-M. and J.S.G. gratefully acknowledge the support by an NSF Grant EAR0911094 and NASA Grant NNX10AG41G. Constructive reviews by Ke Zhang and Michael Bland immensely helped improve the original manuscript. We appreciate the insightful comments and suggestions from Francis Nimmo, Dan Lathrop, and Bill McDonough.

Appendix A. Numerical techniques

In this model, thickness of the conductive ice shell grows with time, while the ocean shrinks by freezing. The nature of the moving boundary in the problem requires special attention to a few details. First, the moving boundary leads to adaptive remeshing in order to keep the model resolution reasonable. Secondly, the freeze rate in Eq. (8) becomes near zero if the initial ice shell thickness and initial ice shell heat flux are both small or near zero (Mitchell and Vynnycky, 2009). To address both of these issues, we employed the Boundary Immobilization Method (BIM) (Caldwell and Kwan, 2004; Mitchell and Vynnycky, 2009). In the adaptive BIM, we make the substitution,

$$z' = \frac{z}{h}, \tag{A.1}$$

to solve Eqs. (7) and (8). After making the substitution, Eqs. (7) and (8) can be rewritten in terms of a new function $f(t) = h^2$,

$$f\frac{\partial T_{ice}}{\partial t} = \frac{z'}{2}\frac{\mathrm{d}f}{\mathrm{d}t}\frac{\partial T_{ice}}{\partial z'} + \frac{\partial^2 T_{ice}}{\partial z'^2} + f\psi, \tag{A.2}$$

$$\frac{\mathrm{d}f}{\mathrm{d}t} = 2\mathcal{S}t\left(\frac{\partial T_{ice}}{\partial z'}\right)_{z'=1} - 2\sqrt{f}q_{rad}(t)\Big|_{z'=1}. \tag{A.3}$$

Following the technique outlined by Mitchell and Vynnycky (2009), we discretize Eqs. (A.2) and (A.3) implicitly in temperature and explicitly in ice shell thickness. The discretized equations, centered on the ith node of a linear grid at the nth time step, can be written as,

$$\begin{aligned} f^n\left(T_i^n + \psi_i^n\right) = &-\frac{\Delta t}{\Delta z^2}\left[\frac{\Delta z}{4}z'\left(\frac{\mathrm{d}f}{\mathrm{d}t}\right)^n + 1\right]T_{i+1}^{n+1} \\ &\times \frac{\Delta t}{\Delta z^2}\left[\frac{\Delta z}{4}z'\left(\frac{\mathrm{d}f}{\mathrm{d}t}\right)^n - 1\right]T_{i-1}^{n+1} \\ &+ \left[\frac{2\Delta t}{\Delta z^2} + f^n\right]T_i^{n+1}, \end{aligned} \tag{A.4}$$

$$f^{n+1} = f^n + \frac{\mathcal{S}t\Delta t}{\Delta z}\left[3T_M^n - 4T_{M-1}^n + T_{M-2}^n\right] - 2\Delta t\sqrt{f^n}q_{rad}(t). \tag{A.5}$$

The first discretized equation leads to a tridiagonal system of linear equations, which was solved using subroutines from LAPACK library implemented via the intel Math Kernel Library. We also tested the sample problem of freezing of a planar interface discussed by Mitchell and Vynnycky (2009) and Caldwell and Kwan (2004) to benchmark our numerical results (Gaeman, 2011).

References

Agnor, C.B., Hamilton, D.P., 2006. Neptune's capture of its moon Triton in a binary-planet gravitational encounter. Nature 441, 192–194.

Biot, M.A., 1954. Theory of stress–strain relationships in anisotropic viscoelasticity and relaxation phenomena. J. Appl. Phys. 25, 1385–1391.

Brada, M.P., Clarke, D.R., 1997. Thermodynamic approach to the wetting and dewetting of grain boundaries. Acta Mater 45, 2501–2508.

Brown, R.H., Kirk, R.L., 1994. Coupling of volatile transport and internal heat flow on Triton. J. Geophys. Res. 99, 1965–1981.

Brown, R.H., Johnson, T.V., Goguen, D.J., Schubert, G., Ross, M.N., 1991. Triton's global heat budget. Science 251, 1465–1467.

Caldwell, J., Kwan, Y., 2004. Numerical methods for one-dimensional Stefan problems. Commun. Numer. Methods Eng. 20, 535–545.

Chan, J.P., Giauque, W.F., 1964. The entropy of nh3-2h2o. Heat capacity from 15 to 300 k. J. Phys. Chem. 68, 3053–3057.

Choukroun, M., Grasset, O., 2007. Thermodynamic model for water and high-pressure ices up to 2.2 GPa and down to the metastable domain. J. Chem. Phys. 127, 124506-1–124506-11.

Choukroun, M., Grasset, O., 2010. Thermodynamic data and modeling of the water and ammonia–water phase diagrams up to 2.2 GPa for planetary geophysics. J. Chem. Phys. 133, 144502-1–144502-13.

Ćuk, M., Gladman, B.J., 2005. Constraints on the orbital evolution of Triton. Astrophys. J. 626, L113–L116.

Feistel, R., Wagner, W., 2006. A new equation of state for H_2O ice Ih. J. Phys. Chem. Refer. Data 35, 1021–1047.

Gaeman, J., 2011. Crystallization of a Subsurface Ocean on Triton. Master's Thesis. University of Maryland, College Park.

Hinze, M., Ziegenbalg, S., 2007. Optimal control of the free boundary in a two-phase Stefan problem. J. Comput. Phys. 223, 657–684.

Hinze, M., Paetzold, O., Ziegenbalg, S., 2009. Solidification of a GaAs melt-optimal control of the phase interface. J. Crystal Growth 311, 2501–2507.

Hogenboom, D.L., Kargel, J.S., Consolmagno, G.J., Holden, T.C., Lee, L., Buyyounouski, M., 1997. The ammonia-water system and chemical differentiation in icy satellites. Icarus 128, 171–180.

Hussmann, H., Spohn, T., 2004. Thermal orbital evolution of Io and Europa. Icarus 171, 391–410. http://dx.doi.org/10.1016/j.icarus.2004.05.020.

Hussmann, H., Sohl, F., Spohn, T., 2006. Subsurface oceans and deep interiors of medium-sized outer planet satellites and large trans-neptunian objects. Icarus 185, 258–273.

Kaula, W.M., 1964. Tidal dissipation by solid friction and the resulting orbital evolution. Rev. Geophys. 2, 661–685.

Lodders, K., 2003. Solar System abundances and condensation temperatures of the elements. Astrophys. J. 591, 1220–1247.

McKinnon, W.B., Kirk, R.L., 2007. Encyclopedia of the Solar System. Academic Press, pp. 483–502 (Chapter Triton).

McKinnon, W.B., Leith, A.C., 1995. Gas drag and the orbital evolution of a captured Triton. Icarus 118, 392–413.

Meyer, J., Elkins-Tanton, L., Wisdom, J., 2010. Coupled thermal–orbital evolution of the early Moon. Icarus 208, 1–10. http://dx.doi.org/10.1016/j.icarus.2010.01.029.

Mitchell, S.L., Vynnycky, M., 2008. Finite-difference methods with increased accuracy and correct initialization for one-dimensional Stefan problems. In: International Workshop on Physics and Computation, Vienna, Austria, August 25–28, Appl. Math. Comput. 215, 1609–1621.

Moore, W.B., Schubert, G., 2000. NOTE: The tidal response of Europa. Icarus 147, 317–319.

Prockter, L.M., Nimmo, F., Pappalardo, R., 2005. A shear heating origin for ridges on Triton. Geophys. Res. Lett., 32.

Roberts, J.H., Nimmo, F., 2008. Tidal heating and long term stability of a subsurface ocean in Enceladus. Icarus 194, 675–689.

Robuchon, G., Nimmo, F., 2011. Thermal evolution of Pluto and implications for surface tectonics and a subsurface ocean. Icarus 216, 426–439.

Ross, M.N., Schubert, G., 1990. The coupled orbital and thermal evolution of Triton. Geophys. Res. Lett. 17, 1749–1752.

Ruiz, J., 2003. Heat flow and depth to a possible internal ocean in Triton. Icarus 166, 436–439.

Sabadini, R., Vermeersen, B., 2004. Global Dynamics of the Earth: Applications of Normal Mode Relaxation Theory to Solid-Earth Geophysics. Kluwer Academic Publishers, Dordrecht, The Netherlands.

Schenk, P., Jackson, M., 1993. Diapirism on Triton: A record of crustal layering and instability. Geology 21, 299–302.

Schenk, P.M., Zahnle, K., 2007. On the negligible surface age of Triton. Icarus 192, 135–149.

Schubert, G., Turcotte, D.L., Olson, P., 2001. Mantle Convection in the Earth and Planets. Cambridge University Press.

Slack, G.A., 1980. Thermal conductivity of ice. Phys. Rev. A 22, 3065–3071.

Solomatov, V., 2007. Magma oceans and primordial mantle differentiation. In: Stevenson, D. (Ed.), Treatise on Geophysics, vol. 9. Elsevier, pp. 91–119, doi:http://dx.doi.org/10.1016/B978-044452748-6.00141-3 (Chapter 9.04).

Tan, L., Zabaras, N., 2007. Modeling the growth and interaction of multiple dendrites in solidification using a level set method. J Comput. Phys. 226, 131–155.

Tobie, G., Mocquet, A., Sotin, C., 2005. Tidal dissipation within large icy satellites: Applications to Europa and Titan. Icarus 177, 534–549. http://dx.doi.org/10.1016/j.icarus.2005.04.006.